A&A 596, A86 (2016)
DOI: 10.1051/0004-6361/201628162

Astronomy & Astrophysics

Study of galaxies in the Lynx-Cancer void

VI. H I-observations with Nançay Radio Telescope★

S. A. Pustilnik[1, 2] and J.-M. Martin[3, 4]

[1] GEPI, Observatoire de Paris, Place Jules Janssen, 92195 Meudon, France
[2] Special Astrophysical Observatory of RAS, Nizhnij Arkhyz, 369167 Karachai-Circassia, Russia
e-mail: `sap@sao.ru`
[3] GEPI, Observatoire de Paris, PSL Research University, CNRS, Univ Paris Diderot, Sorbonne Paris Cité, Place Jules Janssen, 92195 Meudon, France
[4] Station de Radioastronomie de Nançay, Observatoire de Paris, CNRS, 18330 Nançay, France

Received 19 January 2016 / Accepted 26 July 2016

ABSTRACT

Context. Void population consists mainly of late-type and low surface brightness (LSB) dwarf galaxies, whose atomic hydrogen is the main component of their baryonic matter. Therefore observations of void galaxy HI are mandatory to understand both their evolution and dynamics.

Aims. Our aim was to obtain integrated HI parameters for a fainter part of the nearby Lynx-Cancer void galaxy sample (total of 45 objects) with the Nançay Radio Telescope (NRT) and to conduct the comparative analysis of the whole 103 void galaxies with known HI data with a sample of similar galaxies residing in denser environments of the Local Volume.

Methods. For HI observations we used the NRT with its sensitive antenna/receiver system FORT and standard processing. The comparison of the void and "control" samples on the parameter $M(\mathrm{HI})/L_\mathrm{B}$ is conducted with the non-parametric method "The 2 × 2 Contingency Table test".

Results. We obtained new HI data for about 40% of the Lynx-Cancer galaxy sample. Along with data from the literature, we use for further analysis data for 103 void objects. The proxy of the evolutional parameter $M(\mathrm{HI})/L_\mathrm{B}$ of the void sample is compared with that of 82 galaxies of morphological types 8–10 residing in the Local Volume groups and aggregates.

Conclusions. At the confidence level of $P = 0.988$, we conclude that for the same luminosity, these void galaxies are systematically gas-richer, in average by ~39%. This result is consistent with the authors' earlier conclusion on the smaller gas metallicities and evidences for the slower low-mass galaxy evolution in voids.

Key words. galaxies: dwarf – galaxies: evolution – galaxies: distances and redshifts – large-scale structure of Universe – radio lines: galaxies

1. Introduction

Low-mass galaxies are thought to be the most fragile with respect to both internal and external perturbations of various origin (interactions, inflows, mergers) (e.g., Dekel & Silk 1986; Babul & Rees 1992). Therefore it is expected that their evolution is most sensitive to various kinds of galaxy collisions (e.g., distant tidals, close pass-byes, major and minor mergers). Thus, it may significantly depend on the mean galaxy number density of various classes of the Large-Scale structure. Indeed, the strongest effects of dense environment on low-mass galaxy properties are found in galaxy clusters (e.g., Boselli et al. 2014, and references therein). In this scheme, if external perturbations play a substantial role in the secular evolution of typical dwarf galaxies, one expects that at least the part of the dwarf galaxies located in voids could be less evolved objects.

Besides, studies of gravitational instabilities in the cold dark matter cosmology indicate that low-mass haloes become bound later in the underdensity regions (low gravitational potential, e.g. Einasto et al. 2011). This is connected with the appearance of a bias in the gaussian peaks formalism for the structure formation (Bardeen et al. 1986; Dekel & Silk 1986). This, in turn, could also favor the appearance of less evolved low-mass galaxies in voids.

The study of galaxies in voids was quite popular during the last decade (Rojas et al. 2005; Patiri et al. 2006; Sorrentino et al. 2006; Kreckel et al. 2012; Beygu et al. 2012, among others), thanks to the emerging large sky surveys like the SDSS (Sloan Digital Sky Survey) and 2dFGRS (Two-degree field galaxy redshift survey). However, most of the studies of void galaxies mentioned above were mainly devoted to large and rather distant ($D \gtrsim 80{-}100$ Mpc) voids. This last choice, coupled with the demand of statistically complete galaxy samples (based on the apparent magnitude limit), limits the deepness of their void galaxy samples at the level of $M_\mathrm{B}(M_\mathrm{r}) \lesssim -17$.

Some differences between void and wall galaxies in this luminosity range have been noticed. Namely, void objects show higher proportion of blue galaxies and higher star formation rates (SFR) (e.g., Rojas et al. 2004, 2005; and Hoyle et al. 2005, 2012). Similar results were obtained in the recent cosmological simulations by Kreckel et al. (2011), which indicate that effect of global environment of voids and walls is rather subtle for more massive galaxies. They found however evidences

---

★ The reduced spectra (FITS files) are only available at the CDS via anonymous ftp to `cdsarc.u-strasbg.fr` (`130.79.128.5`) or via `http://cdsarc.u-strasbg.fr/viz-bin/qcat?J/A+A/596/A86` that less massive objects in voids can show signs of evolutionary youth.

In order to address the issue of void environment effect on low-mass galaxy evolution (for galaxies below the adequate mass/luminosity limit – e.g., at $M_{\rm B} \sim -12$ or fainter), one needs to study samples of intrinsically faint objects. Having in mind the common apparent magnitude limits of the main wide-angle redshift surveys (equivalent to $B_{\rm tot} \sim$ 18.0–18.5), this implies the necessety to study objects closer than ~20 Mpc, located in the nearby voids which are adjacent to the Local Volume.

In Pustilnik & Tepliakova (2011, Paper I) we described the large galaxy sample in the nearby Lynx-Cancer void ($D_{\rm centre} \sim$ 18 Mpc) and presented their main known parameters. One of the tasks was to measure and analyze the evolutionary parameters of void galaxies: metallicity (or gas-phase O/H) and gas mass-fraction. In the published version, there are 79 galaxies with the absolute magnitudes $M_{\rm B}$ in the range [−12, −18.4], with median of −14.0, and with the substantial incompleteness at the fainter luminosities. Roughly half of the void sample galaxies are Low Surface Brightness (LSB) galaxies, with extinction and inclination corrected central SB values of $\mu_{0,\rm B,i} \geq 23.0^{\rm m}/\square''$.

In Papers II and VII (Pustilnik et al. 2011a, 2016), we present a study of O/H in 77 members of the Lynx-Cancer void sample. We compared the data with the parameter O/H of similar galaxies in denser environments. Void galaxies appear to have systematically lower O/H (by about ~37% in average) for the same luminosities. Other studies show that ~20% of void LSB Dwarf galaxies (Pustilnik et al. 2011b; Chengalur & Pustilnik 2013; Perepelitsyna et al. 2014) turned out very metal-deficient and/or extremely gas-rich, indicating that void environment is "conducive" for unevolved objects.

The major part of late-type dwarf galaxies located in the Lynx-Cancer and presumably in other nearby voids are LSB objects (e.g., Perepelitsyna et al. 2014, hereafter Paper IV). The latter are known to have the significant or dominant part of baryon mass in the form of cold neutral gas. To study the properties of this very important component of void galaxies, one needs to know their global HI parameters and, first of all, their HI mass, in order to derive their second evolutionary parameter, the gas mass-fraction $f_{\rm gas}$. Moreover, since in many void galaxies the neutral gas appears to be the main baryonic component, it is crucial to know its physical properties in order to understand galaxy dynamics and star formation. Unusual, very gas-rich and metal-poor galaxies found in course of HI surveys, are good candidates for detailed HI mapping. Some of studies of very metal-poor dwarfs are presented in papers of Chengalur et al. (2006), Ekta et al. (2006, 2008, 2009).

For half of the void galaxy sample (mainly for the brighter, more massive ones), the global HI parameters were known from various published sources (mainly from Haynes et al. 2011; Springob et al. 2005; Huchtmeier & Richter 1989; Swaters et al. 2002; and Begum et al. 2008). For the remaining void galaxies, we needed to conduct our own HI observations. Thus, the general goal of this work was to perform the most complete study of the void galaxy HI-properties. Besides, having the first results of such study, there was a hope to find new unusual very gas-rich dwarfs among the fainter part of the void objects.

Some very interesting void low surface brightness dwarfs (LSBDs), namely very low metallicity and/or very gas-rich ones were presented in Pustilnik et al. (2010, 2011b), Chengalur & Pustilnik (2013) and Chengalur et al. (2015). As the data in Paper I show, the Lynx-Cancer void galaxies have a rather small radial velocity dispersion. This is interesting by itself in order to confront with cosmological simulations. Also this relates directly to the identification of void filaments. Since HI velocities are in general substantially more accurate than optical ones, they provide an additional opportunity to address the issues mentioned above.

Here we present all the NRT observed galaxies with known radial velocities from the updated (relative to Paper I) void sample (Pustilnik et al. 2016, and in prep.), which currently includes 108 objects satisfying the primary selection criteria of this sample.

2. Sample

In Table A.1 we present the main parameters taken from NED[1], SDSS[2] or from the literature for all observed 45 void galaxies. New objects, taken from the updated Lynx-Cancer void sample (Pustilnik et al. 2016, and in prep.) are marked by an asterisk (as well as in Table A.3). Table A.1 is organized as follows: Col. 1 – short IAU-style name, Col. 2 – other name or prefix (SDSS, HIPASS, etc.), Col. 3 – galaxy type, Cols. 4 and 5 – Epoch J2000 RA and Declination, Col. 6 – heliocentric velocity from optical data (when available), Col. 7 – heliocentric velocity from HI data, Col. 8 – total *B*-band magnitude. In most of the cases, this value is calculated from the total *g* ad *r* magnitudes following Lupton et al. (2005). The latter values are obtained in Paper IV on the photometry of the SDSS DR7 (Abazajian et al. 2009) images. For galaxies located outside of the SDSS footprint, the *B*-band magnitudes are adopted from Pustilnik & Tepliakova (2011) where respective references are given. The only exception is J0802+0525 for which its *B*-magnitude is estimated directly from its SDSS model *g* and *r* values since due to a nearby bright star we were unable to perform own photometry, Col. 9 – respective absolute magnitude, corrected for the Galaxy extinction $A_{\rm B}$ according to Schlafly & Finkbeiner (2011). The adopted distances are based on heliocentric velocities V(HI) from Table A.2. They are calculated according to the prescriptions given in Paper I, accounting for the large peculiar velocity in this region $\Delta V \sim -300$ km s^{-1} (Tully et al. 2008). For a few objects, distances were determined using the velocity-independent (mainly Tip of RGB) methods. In Col. 10 we give a galaxy alternative name.

3. Observations and reduction

The HI observations were made during the period 2007–2013 with the Nançay Radio Telescope (NRT). The NRT has a collecting area of 200×34.5 m and a half-power beam width (HPBW) of 3.7′ (East-West) × 22′ (North-South) at 21-cm and for a declination of $\delta = 0^\circ$ [3]. A cooled 1.1−1.8 GHz dual-polarization receiver and a 8192 channel autocorrelation spectrometer were used for the observation of the HI line. The system temperature was about 35 K and the conversion factor of the antenna temperature to the flux density for a point source was 1.5 K Jy^{-1} near equator. The spectrometer covered a velocity range of about 2700 km s^{-1}, providing a channel spacing of 1.3 km s^{-1} before smoothing. The effective resolution after averaging of four adjacent channels and Hanning smoothing was ≈10.4 km s^{-1}. Observations were obtained in separate cycles of "ON-source" and "OFF-source" integrations, each of 40 or 60 s in duration. "OFF"

---

[1] NASA/IPAC Extragalactic Database (NED).

[2] Sloan Digital Sky Survey (Abazajian et al. 2009, and references therein).

[3] See `http://nrt.obspm.fr`

integrations were acquired at the target declination, with RA offset of ~15′ × cos(δ) to the East.

A noise diode has been used to perform flux density calibration. Its power was regularly monitored through the observations of known continuum and line sources. The comparisons of our measured fluxes with independent measurements of the same objects with other telescopes indicates that flux density scales are consistent within 10%.

With the rms noise of ~1.5 to 5 mJy per resolution element after smoothing (10.4 $\mathrm{km\,s^{-1}}$), we achieved a S/N ratio for the peak flux densities F_{peak} of the detected galaxies of 20–30 for the brightest objects, while for the faintest sources we had detections with a S/N ratio of only ~2.5–4. Total integration times per galaxy ("ON" + "OFF" + pointing time) varied between 0.6 and 6 h. For three of the forty five observed Lynx-Cancer void galaxies we obtained only upper limits of their F_{peak} and of their HI flux.

Primary data reduction has been made with the standard NRT program *NAPS* written by the telescope's staff. The follow-up data processing has been done with the IRAM package *CLASS*. Both horizontal and vertical polarization spectra were calibrated and processed independently. They were finally averaged together. The baselines were generally well-fitted by a third order or lower polynomial and were subtracted out. Comments on the noise estimates and on several marginally detected or undetected void galaxies of 45 observed are given in the next section.

4. Results

Table A.2 presents the HI parameters derived from the observations. This is organized as follows: Col. 1 – short IAU-style name, Col. 2 – heliocentric velocity of the detected HI line with its 1σ error, in $\mathrm{km\,s^{-1}}$. This is determined as the midpoint between the half-peak points on both sides of the HI profile; Col. 3 – the adopted distance as in Paper I (see comment for Col. 9 in Table A.1); Cols. 4 and 5 – velocity widths in $\mathrm{km\,s^{-1}}$ of the HI profile at 50% and 20% of peak, W_{50}, W_{20} with their 1σ errors. They are determined as the velocity range between the respective points on both sides of the HI profile; Col. 6 – F(HI) – integrated flux of detected HI signal with its 1σ error in $\mathrm{Jy\,km\,s^{-1}}$. Formulae for error estimates of parameters in Cols. 2, 4–6 were adopted from our earlier NRT HI-survey (Thuan et al. 1999) which in turn uses the prescriptions from Schneider et al. (1990); Col. 7 – logarithm of total mass M(HI), in units of solar mass with its 1σ error; Col. 8 – ratio of $M(\mathrm{HI})/L_{\mathrm{B}}$ with related 1σ error, in solar units; Col. 9 – total time ON-source in minutes; Col. 10 – rms of noise near the HI peak in mJy at the velocity resolution of 10.4 $\mathrm{km\,s^{-1}}$; Col. 11 – Signal-to-Noise ratio for peak value of the respective HI profile.

Figure 1 shows in order of increasing RA the HI profiles of the void galaxies listed respectively in Tables A.1 and A.2. For the triplet of MRK 407 (J094747.60+390503.0) only two HI profiles are presented, which are rather complex and have been obtained with the NRT beam pointing in the direction of the largest members of the triplet. In addition, HI profile of the galaxy J090018.30+322226.2 is not shown, since no signal have been detected. Therefore, the total number of profiles displayed is 43. We present below our comments about some peculiar objects.

SDSS J072301.42+362117.1 and *J072313.46+362213.0*. The first galaxy, a LSB dwarf, has been identified as a new Lynx-Cancer void galaxy after its redshift was obtained at the SAO 6 m telescope (BTA). Its NRT HI profile suggested a possible contribution from a nearby galaxy which has been found as a very low surface brightness dwarf, ~2$^{\mathrm{m}}$ fainter than the main component, at ~3′ to E (J072313.46+362213.0). An additional NRT observation in the direction allowed to partly disentangle the confusion between the HI contributions. The final HI parameters for these two galaxies and a third one even fainter (J072320.57+362440.8, see Table A.3) have been adopted after the subsequent GMRT HI mapping of this triplet (Chengalur & Pustilnik 2013).

SDSS J080238.15+052551.2. This very faint and compact optical object close to a bright star was included to the void sample after its assumed identification with a faint ALFALFA source (Haynes et al. 2011) with $V(\mathrm{HI}) = 830\ \mathrm{km\,s^{-1}}$, $F(\mathrm{HI}) = 0.43 \pm 0.04\ \mathrm{Jy\,km\,s^{-1}}$ with S/N ratio of 6.2 (AGC 188988). With such parameters, this galaxy has a very high ratio $M(\mathrm{HI})/L_{\mathrm{B}} \sim 4.8$ (using the total SDSS g and r magnitudes, transformed to $B_{\mathrm{tot}} = 19.8$). Since very gas-rich galaxies are rare objects, we conducted HI observations of AGC 188988 with the NRT. Our NRT data indicate no signal at the respective velocity with an upper limit of $F(\mathrm{HI}) < 0.16\ \mathrm{Jy\,km\,s^{-1}}$ (2σ).

The probable interpretation of this case is a false ALFALFA detection. If however there exists HI associated with the suggested faint optical object, its ratio $M(\mathrm{HI})/L_{\mathrm{B}} < 1.8$ is not so large. We consider this object's data as unreliable and excluded it from the following statistical analysis.

SDSS J090018.30+322226.2. This galaxy is a new void object with $V_{\mathrm{hel}} = 740 \pm 30\ \mathrm{km\,s^{-1}}$, as measured on the faint Hα emission in the spectrum obtained at the BTA. At NRT the signal at this radial velocity is within 1.4σ, so the numbers below should be treated as upper limits. With $W_{50} = 30\ \mathrm{km\,s^{-1}}$, typical of galaxies with $M_{\mathrm{B}} \sim -12$, that results in the total flux of $0.14 \pm 0.10\ \mathrm{Jy\,km\,s^{-1}}$. For parameter $M(\mathrm{HI})/L_{\mathrm{B}}$ the respective value is 0.72 ± 0.52.

SDSS J094003.27+445931.7. This galaxy has marginally detected HI with the radial velocity close to that derived from the SDSS emission-line spectrum ($1358 \pm 4\ \mathrm{km\,s^{-1}}$). However, there is also a similar flux detection (at the level of ~(2–3)σ) at $V_{\mathrm{hel}} = 1202 \pm 8\ \mathrm{km\,s^{-1}}$. The search for a possible optical counterpart on the SDSS image to this HI component produced two candidates within the NRT beam.

The nearest one is a small and almost edge-on blue disc SDSS J093951.28+445921.9 with $g = 19.34$, $r = 19.15$. Its BTA spectrum have revealed the velocity of Hα line of ~14 000 $\mathrm{km\,s^{-1}}$. The second candidate is the almost face-on LSB disc SDSS J093950.11+444800.1 with $g = 17.55$, $r = 17.18$ ($B \sim 17.90$), ~11.5′ to the S and 13.16 s (~140″) to the W. Due to the NRT beam offset, its nominal HI-flux should drop by a factor of 6.5. In this case, its ratio $M(\mathrm{HI})/L_{\mathrm{B}}$ is ~1.4, rather typical of void LSBDs. The optical redshift of this galaxy is needed, in order to fix the origin of the second HI source.

MRK 407 = J094747.60+390503.0. This blue compact galaxy (BCG) is the brightest member of a triplet which includes also ~1.7-mag fainter LSBD UZC J09475+3908 at 3′ to N and ~3-mag fainter LSBD SDSS J094758.45+390510.1 at ~2′ to E. Each galaxy contributes to the F(HI) for any NRT pointing in the direction of the triplet. We used our NRT results, accounting for the "a priori" known decrease of HI flux for the sources NRT beam offset, as well as the earlier observations of MRK 407 by Thuan & Martin (1981) to disentangle the contribution of each component of the triplet. The typical estimated accuracy of the resulted F(HI) is ~20%. Follow-up GMRT mapping of this triplet (Chengalur et al., in prep.) will give a better understanding of its properties.

SDSS J095633.65+271659.3 with $V_{\mathrm{hel}} = 1059\ \mathrm{km\,s^{-1}}$ is a faint companion of a ~4$^{\mathrm{m}}$ brighter spiral IC 2520 (at 13.2$^{\mathrm{s}}$ to W and 3.3′ to S, see Table A.3), which is also in the NRT beam and

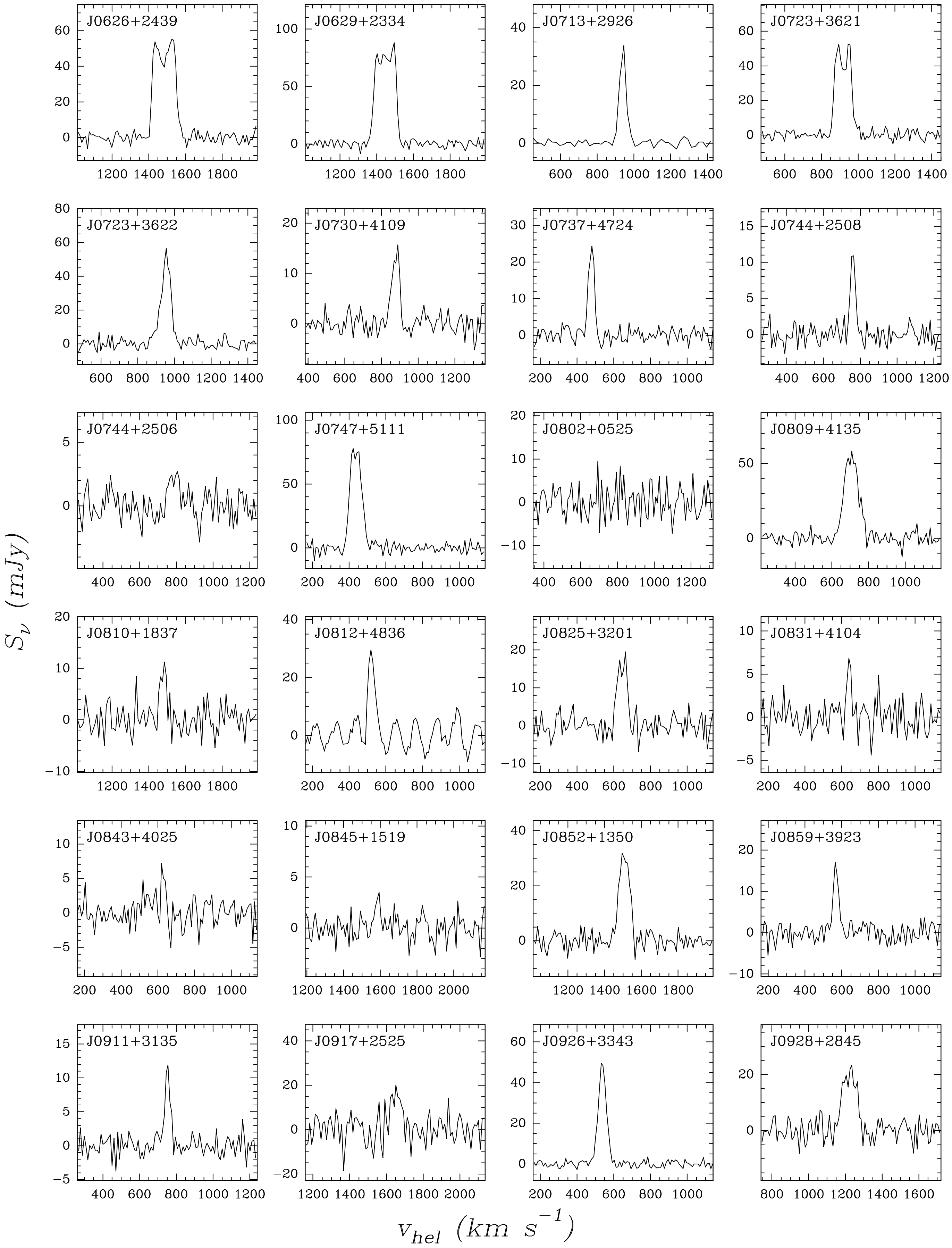

Fig. 1. The NRT HI profiles S_ν (in mJy) vs. $V_{\rm hel}$ (km s^{-1}) of all studied galaxies.

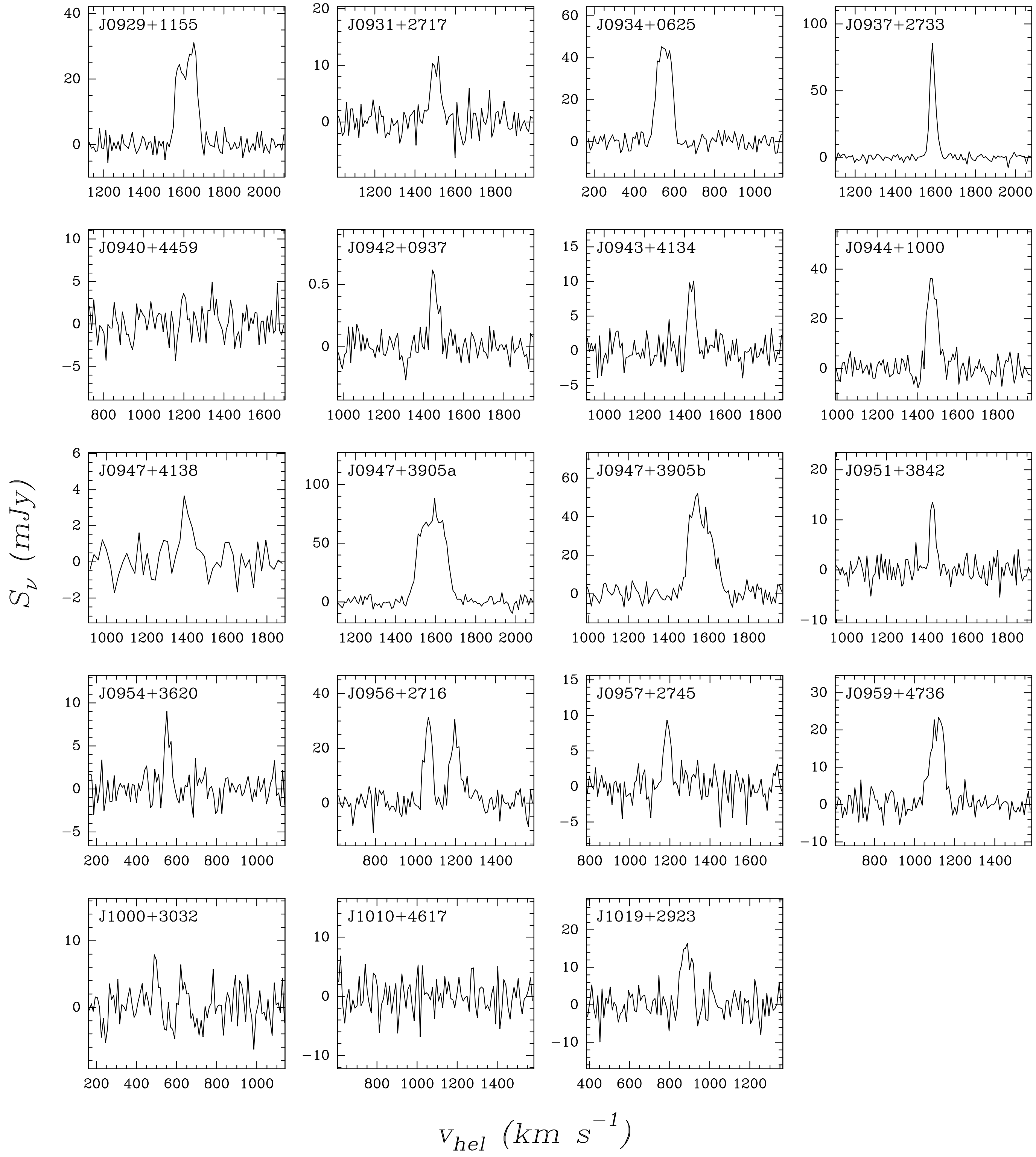

Fig. 1. continued.

is seen in the plot of HI profile as an additional peak at $V_{\rm hel}$ = 1243 km s^{-1}.

SDSS J101014.96+461744.1. This is a faint galaxy with a good S/N SDSS emission-line spectrum. Its optical redshift corresponds to $V_{\rm hel}$ = 1092 ± 3 km s^{-1}. On our data, there is no detectable HI flux, for $\sigma_{\rm noise} \sim 2.4$ mJy. For statistical analysis, we adopt for its F the upper limit F(HI) < 0.12 Jy km s^{-1} and the value of M(HI)/$L_{\rm B}$ < 0.34.

5. Analysis

In our analysis of the properties of the Lynx-Cancer void galaxy sample, we use the optical parameters gathered from the literature, as mentioned previously in Sect. 2, and the HI parameters obtained from our observations or taken from the literature. Table A.3 lists galaxies with HI data taken from the literature, with their HI and optical parameters. Table A.3 is organized as follows: Cols. 1 to 5 – same as Table A.1; Col. 6

Table 1. The 2 × 2 Contingency Table test.

Property	G	non-G	Sum 1
V	$m = 61$	$n - m = 42$	$n = 103$
non-V	$M - m = 34$	$N - n - (M - m) = 48$	$N - n = 82$
Sum 2	$M = 95$	$N - M = 90$	$N = 185$

– adopted heliocentric velocity $V_{\rm hel}$; Cols. 7 and 8 – the total apparent and absolute B magnitudes: for the published sample outside the SDSS zone – from Paper I, for galaxies with new photometry – from papers by Perepelitsyna et al. (2014) and for the rest of the updated version of the void sample – from Pustilnik et al. (2016, and in prep.). Few exceptions are the following. For J0706+3620 and UGC 3672, their B magnitudes are adopted from Chengalur et al. (2016). For J0736+0959, its B magnitude is adopted from the recent photometry in Haurberg et al. (2015). For J0956+2900 (DDO68C), there is no possibility to estimate its optical flux due to a nearby bright star. We adopt its B magnitude based on M(HI) in Cannon et al. (2014) and a typical of this sample value of $M({\rm HI})/L_{\rm B} = 1$; Cols. 9 and 10 – total HI flux F(HI) and derived M(HI); Col. 11 – reference to the HI data. In total, we use the data of 103 void galaxies in this analysis.

In order to compare the "gas-content" parameter $M({\rm HI})/L_{\rm B}$ of the void sample with that a sample of galaxies in denser environments, we created a sample of 82 late-type dwarf and subluminous galaxies in the Local Volume (LV) residing in groups and the Canes Venatici I (CVnI) cloud. The latter were described by Karachentsev (2005). We used those members of these groups for which we found HI data in the literature, mainly in the Catalog of Nearby Galaxies (CNG) by Karachentsev et al. (2004).

In Fig. 2 we show (left-hand top and bottom panels, respectively) the distributions of parameter $M({\rm HI})/L_{\rm B}$ for the void and LV-groups sample. The median value of $M({\rm HI})/L_{\rm B}$ for the combined void and LV-group sample of 185 galaxies is equal to 1.01. Therefore galaxies with $M({\rm HI})/L_{\rm B} \geq 1.0$ we call "gas-rich". Despite each sample showing rather large scatter (indicating that there are several affecting factors), the distribution of the void galaxies is confidently shifted to the higher values of $M({\rm HI})/L_{\rm B}$. This effect is apparent in a factor of ~1.39 difference between their medians (1.21 and 0.87, respectively) and the significant difference in fractions of gas-rich objects in the void and LV-groups samples (0.59 and 0.41, respectively). Since these differences might be due to the statistical scatter, more advanced statistical tests are needed.

The significance of the second difference can be tested via non-parametric statistical methods. In particular, we use a test well known in biology and quality control, called "The 2 × 2 Contingency Table test" (e.g., Bol'shev & Smirnov 1983, and references therein). It appears to be more powerful than the Kolmogorov-Smirnov test in problems like this, as was tested for a similar astronomical problem in Pustilnik et al. (1995, see the detailed appendix). Here we briefly summarize the process of groupping the galaxies for the respective cells of Table 2 × 2. The zero hypothesis H_0 states that the property G to be "gas-rich" does not relate to the property V to belong to the void environment, or in other words, the fraction of gas-rich galaxies is the same for both compared samples of late-type galaxies. The respective numbers in cells of Table 2 × 2 are shown in Table 1.

Here $m = 61$ is the number of void gas-rich galaxies and $n - m = 42$ – the number of void non-gas-rich objects. $M - m = 34$ is the number of non-void gas-rich galaxies, while $N - n - (M - m) = 48$ – the number of non-void non-gas-rich ones. If properties G and V were independent, that is there were no correlation between the property to belong to void and the property to be gas-rich, the probability to get accidently the table with the same occupation numbers [61, 42, 34, 48], calculated according to the formulae in the above appendix (and Bol'shev & Smirnov 1983), is less than $p = 0.012$. The respective probability to reject H_0 with the given occupation numbers is $P = 1 - p = 0.9882$. Hence, the visual impression on the significantly higher fraction of void gas-rich objects is supported with the statistical criterion at the confidence level P of 0.9882.

Apart the distributions on parameter $M({\rm HI})/L_{\rm B}$, we also compare in right-hand panels of Fig. 2 its relation to galaxy luminosity (via parameter $M_{\rm B}$). For aid to eye, we draw upper boundary straight lines for both samples. The visual inspection shows that for the Lynx-Cancer void galaxies this upper line goes slightly higher (by a factor of 1.6–2.0) than for "group" galaxies in the whole range of galaxy luminosities. The same is valid for the bottom boundary. With only one exception, the most gas-poor void galaxies have substantially higher values of $M({\rm HI})/L_{\rm B}$ than the similar galaxies in groups.

6. Discussion

In discussing noticeable differences in the gas content between void and "group" late-type galaxies, it is important to pay attention that the "group" sample is itself quite inhomogeneous, including along the classical Local Volume groups similar to our own Local Group (M 81, CenA, M 83, IC 342, Maffei, Scu) one rather rarefied and unrelaxed aggregate known as the CVnI cloud. It is curious and instructive that three of the six most gas-rich galaxies in the "group" sample ($M({\rm HI})/L_{\rm B} = 4.3$–$6.9$) belong to the outer parts of this aggregate, and hence, can be treated as falling to this from the lower-density environment. These most gas-rich galaxies include DDO 154, UGCA 292 and UGC 3741 with respective values of parameter $M({\rm HI})/L_{\rm B}$ of 4.5, 6.9 and 4.3 (see the fresh summary in Chengalur & Pustilnik 2013). The structure of CVnI cloud was revisited by Makarov et al. (2013), based on the improved TRGB distance determinations.

The mentioned above extreme members of CVnI cloud reside far from the centre of the cloud, closer to the zero-velocity radius ($R = 1.06$ Mpc) or substantially further (at ~1.1, 0.9 and 1.6 Mpc, respectively), and thus can probably be treated as being in the process of fall-off onto CVnI cloud. Coming from the significantly lower density environment, they can posess properties of some the most unevolved representatives of underdense regions.

To check the effect of the CVnI cloud galaxies on the comparison of the LV vs. Lynx-Cancer void galaxy samples, we have removed the 11 CVnI cloud galaxies from the whole Local Volume sample. Thus, it left 71 LV galaxies. We apply the same Table 2 × 2 method as above to check the Null hypothesis H_0 on the independence of gas-rich galaxy fraction on the type of environment. For the new table, the probability to get accidently the variant with occupation numbers [61, 42, 27, 44] is $p = 0.00444$, ~2.7 times smaller than for the whole Local Volume subsample. The respective confidence level to reject H_0 is $P = 1 - p = 0.99556$. This probably indicates that at least a part of the CVnI cloud galaxies are in a special evolutionary status.

One important note relates to the conclusion on the difference in distributions of parameter $M({\rm HI})/L_{\rm B}$ for the void and "group" (LVG, Local Volume Groups) samples. As one can see in the right-hand panels of Fig. 2, there is a trend (known also

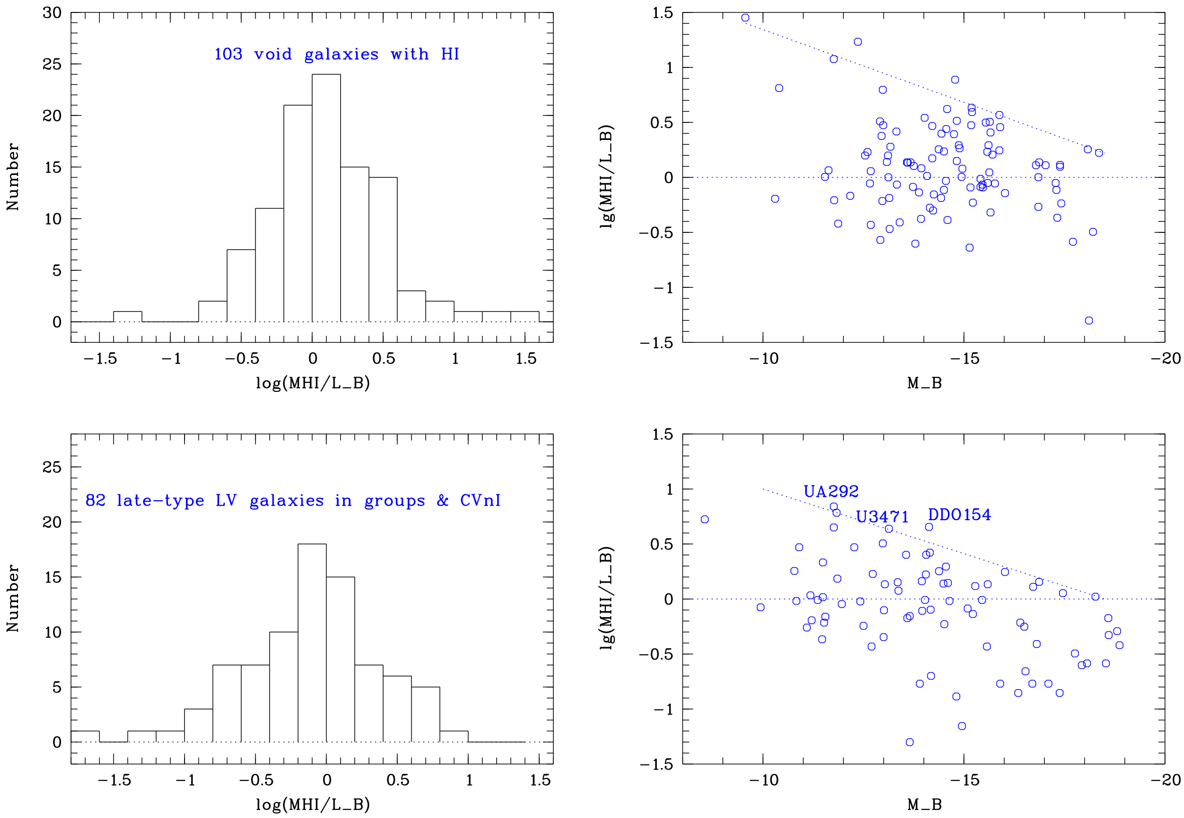

Fig. 2. *Top left*: distribution of mass-to-light ratio $M(\mathrm{HI})/L_{\mathrm{B}}$ for all Lynx-Cancer void galaxies with HI data. *Top right*: the relationship between $M(\mathrm{HI})/L_{\mathrm{B}}$ and the absolute magnitude M_{B}. *Bottom left*: distribution of $M(\mathrm{HI})/L_{\mathrm{B}}$ for late-type dwarf and subluminous galaxies in the Local Volume (LV) groups and the CVnI cloud from Karachentsev (2005). *Bottom right*: the relationship between $M(\mathrm{HI})/L_{\mathrm{B}}$ and the absolute magnitude M_{B} for the same late-type galaxy sample. The scatter of parameter $M(\mathrm{HI})/L_{\mathrm{B}}$ is large for all values of M_{B}, indicating the interplay of several significant factors. Nevertheless, the fraction of higher $M(\mathrm{HI})/L_{\mathrm{B}}$ ratio objects is clearly larger for void galaxies. Also, the three highest ratio galaxies from the LV sample are situated in the outer parts of groups and CVnI cloud (marked by their names). Median values of $M(\mathrm{HI})/L_{\mathrm{B}}$ are respectively, 1.21 and 0.87 for void and the LV "late-type in groups" samples, which differ by a factor of ~1.39. Upper boundary line for the void sample also is a factor of 1.6−2 higher than that for the "group" sample.

from several earlier works, see e.g. Huchtmeier et al. 1997; Pustilnik et al. 2002): the ratio $M(\mathrm{HI})/L_{\mathrm{B}}$ raises with the decrease of galaxy luminosity. See also Fig. 4 for the rate of this increase. Therefore, if the two samples under comparison differ significantly in M_{B} distribution, one can obtain a noticeable difference in distribution $M(\mathrm{HI})/L_{\mathrm{B}}$, even though in reality these samples have the same distribution. In Fig. 3 and with related numbers we show that this is not the case. Indeed, both distributions on M_{B} are rather similar, have close mean and median values of M_{B} (see numbers in the figure legend), and for the "group" sample they are somewhat lower. The latter should lead in general to the opposite effect, that is the "group" sample should have more numerous gas-rich galaxies.

In Fig. 4 we show how the galaxy hydrogen mass $M(\mathrm{HI})$ is related to the blue luminosity L_{B}. The left panel is for the sample of 103 Lynx-Cancer void galaxies, while the right one is for 82 galaxies of the Local Volume group sample. Dotted lines show positions of galaxies with $M(\mathrm{HI})/L_{\mathrm{B}} = 1$ (in solar units, with a slope of 1.0). The red dashed lines (see figure's legend) show the real linear regression for considered samples. They indicate that for both samples, galaxies become on average gas-richer with decreasing luminosity. The respective coefficients in the relation $\log(M(\mathrm{HI})/L_{\mathrm{B}})/\log(L_{\mathrm{B}}) = -0.129 \pm 0.054$ (void sample) and -0.208 ± 0.051 (Local Volume sample) do not differ significantly. Thus, their average $\langle k \rangle = -0.163 \pm 0.040$ can be considered as a representative of such relationship for both samples.

It is interesting to compare this result with estimates published for other samples. In particular, Staveley-Smith et al. (1992) found $k = -0.3 \pm 0.1$ for a sample of LSB dIs and BCGs, while Smoker et al. (2000) found $k = -0.2 \pm 0.1$ for emission-line galaxies of the University of Michigan survey. In the Pustilnik et al. (2002) study of BCGs in various environments, this slope for non-cluster BCGs is consistent with average of $\langle k \rangle = -0.25 \pm 0.1$. Thus, within rather large scatter, all available data for late-type and BCG galaxies on the relation $M(\mathrm{HI})/L_{\mathrm{B}} \propto L_{\mathrm{B}}^{k}$ are consistent with the common index $k \sim -0.2$. This corresponds to the increase of $M(\mathrm{HI})/L_{\mathrm{B}}$ by factor of ~4 for luminosity decrease by a factor of 1000.

This relation is a specific illustration of the well known "down-sizing phenomenon" which is connected to the slower evolution of smaller mass galaxies. The general trend towards lower gas metallicity for smaller galaxies is a better known manifestation of the same phenomenon.

6.1. Summary

1. The NRT HI data are presented for 45 galaxies of the Lynx-Cancer void. Along with HI data already published in the literature, we could build a large sample of 103 galaxies and

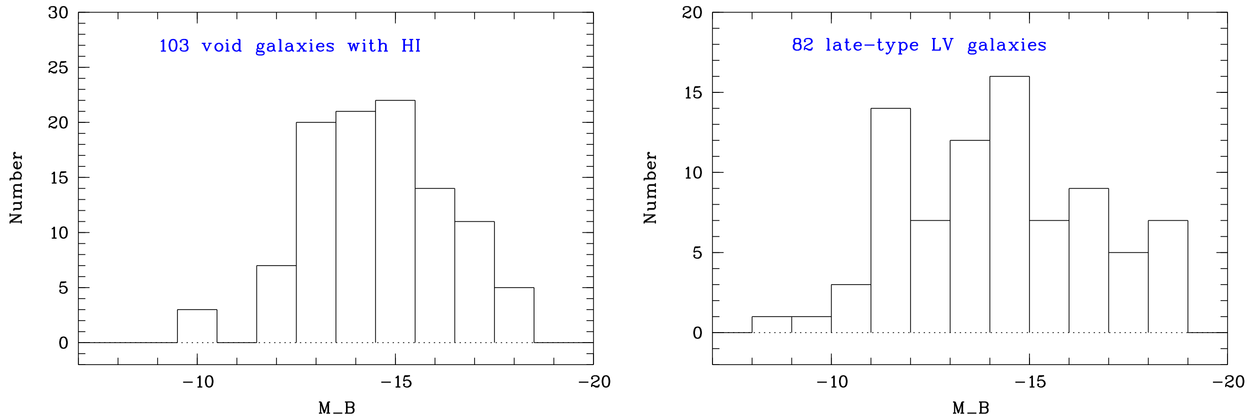

Fig. 3. *Left*: distribution of $M_{\rm B}$ for 103 Lynx-Cancer void galaxies with HI data. *Right*: same distribution of $M_{\rm B}$ for the comparison sample 82 galaxies in groups inside the Local Volume. Median and mean values of $M_{\rm B}$ of the "groups" sample (−14.10 and −14.24) are somewhat fainter than for the void sample (−14.45 and −14.61, respectively). The standard deviation in opposite is somewhat higher (2.38 mag vs. 1.83 mag). See "Discussion" for further implications.

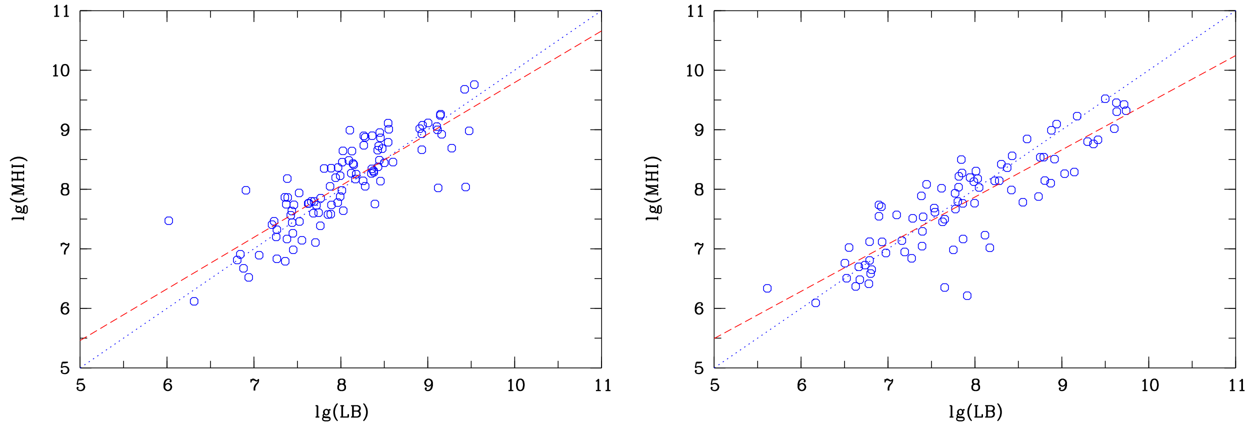

Fig. 4. *Left*: relation between M(HI) and $L_{\rm B}$ (in solar units) for 103 Lynx-Cancer void galaxies with HI data. Dotted line shows positions for objects with M(HI)/$L_{\rm B}$ = 1. Dashed line shows the linear regression on all galaxies, with the slope of $k1 = 0.875 \pm 0.055$ and rms = 0.45 (in log M(HI)). *Right*: same relation for all 82 galaxies from comparison sample in the Local Volume groups. The slope of the linear regression is $k2 = 0.792 \pm 0.051$ and rms = 0.44 (in log M(HI)). See "Discussion" for further implications.

study the properties of $\sim$95% of the updated Lynx-Cancer void galaxy sample.

2. The analysis of parameter M(HI)/$L_{\rm B}$ – observational proxy of the relative gas content – for the void galaxy sample revealed a significant excess (at the confidence level P = 0.988) of gas-rich objects in the void sample with respect to similar late-type galaxies residing in the Local Volume (LV) groups and in the CVnI cloud. For the LV group objects which do not belong to the CnVI cloud, the difference is significant at the confidence level of 0.9956.
3. The latter result can be treated as an independent evidence for slower evolution of typical void galaxies. This is consistent with similar conclusions previously published by the authors, based on the analysis of gas-phase metallicity in void galaxies and similar galaxies in denser environments.
4. The ratio M(HI)/$L_{\rm B}$ for the void galaxies has a broad distribution with extreme values of $\sim$0.05 and $\sim$28, indicating that various competing factors can define the galaxy evolution in voids. The median value of M(HI)/$L_{\rm B}$ varies with $M_{\rm B}$ within a factor of $\sim$4 (from $\sim$0.5 to $\sim$2) for a luminosity range of $\sim$3 orders of magnitude.

Acknowledgements. We thank the NRT Program Committee for allocating time for this project during years 2007–2012. The authors appreciate the anonymous referee's report which allowed to improve the quality of the paper. The work of S.A.P. was partly supported by RFBR grants Nos. 11-02-00261 and 14-02-00520. S.A.P. appreciates the hospitality and support from Paris Observatory and its laboratory GEPI during his visits for this project. We thank J. Chengalur for permission to use HI-fluxes for UGC 3672 system components prior publication. The Nançay Radio Observatory is the Unite scientifique de Nançay of the Observatoire de Paris, associated as Unite de Service et de Recherche (USR) No. B704 to the French Centre National de la Recherche (CNRS). The Nançay Observatory also gratefully acknowledges the financial support of the Conseil Regional de la Region Centre in France. This research has made use of the NASA/IPAC Extragalactic Database (NED) which is operated by the Jet Propulsion Laboratory, California Institute of Technology, under contract with the National Aeronautics and Space Administration. We acknowledge the usage of the HyperLeda database (`http://leda.univ-lyon1.fr`, Paturel et al. 2003).

References

Abazajian, K. N., Adelman-McCarthy, J. K., Agüeros, M. A., et al. 2009, ApJS, 182, 543
Babul, A., & Rees, M. J. 1992, MNRAS, 255, 346
Bardeen, J. M., Bond, J. M., Kaiser, N., & Szalay, A. S. 1986, ApJ, 304, 15
Begum, A., Chengalur, J. N., Karachentsev, I. D., Sharina, M. E., & Kaisin, S. S. 2008, MNRAS, 386, 1667
Beygu, B., Kreckel, K., van de Weygaert, R., van der Hulst, J. M., & van Gorkom, J. H. 2012, AJ, 145, 120
Bol'shev, L. N., & Smirnov, N. V. 1983, Tables of Mathematical Statistics (Moscow: Nauka Publishers)
Boselli, A., Voyer, E., Boissier, S., et al. 2014, A&A, 570, A69
Cannon, J. M., Johnson, M., McQuinn, K., et al. 2014, ApJ, 787, L1

Chengalur, J. N., & Pustilnik, S. A. 2013, MNRAS, 428, 1579
Chengalur, J. N., Pustilnik, S. A., Martin, J.-M., & Kniazev, A. Y. 2006, MNRAS, 371, 1849
Chengalur, J. N., Pustilnik, S. A., Makarov, D. I., et al. 2015, MNRAS, 448, 1643 (Paper V)
Chengalur, J. N., Pustilnik, S. A., & Egorova, E. S. 2016, MNRAS, in press
Dekel, A., & Silk, J. 1986, ApJ, 303, 39
Einasto, J., Suhhonenko, I., Hutsi, G., et al. 2011, A&A, 534, A128
Ekta, C., Jayaram, N., & Pustilnik, S. A. 2006, MNRAS, 372, 853
Ekta, C., Jayaram, N., & Pustilnik, S. A. 2008, MNRAS, 391, 881
Ekta, B., Pustilnik, S. A., & Chengalur, J. N. 2009, MNRAS, 397, 963
Haurberg, N. C., Salzer, J. J., Cannon, J. M., & Marshall, M. V. 2015, ApJ, 800, 121
Haynes, M., Giovanelli, R., Martin, A. M., et al. 2011, AJ, 142, 170
Hirschauer, A. S., Salzer, J. J., Skillman, E. D., et al. 2016, ApJ, 822, 108
Hoyle, F., Rojas, R. R., Vogeley, M. S., & Brinkmann, J. 2005, ApJ, 620, 618
Hoyle, F., Vogeley, M. S., & Pan, D. 2012, MNRAS, 426, 3041
Huchtmeier, W. K., & Richter, O.-G., A General Catalog of HI Observations of Galaxies (New York: Springer-Verlag)
Huchtmeier, W. K., Hopp, U., & Kuhn, B. 1997, A&A, 319, 67
Karachentsev, I. D. 2005, AJ, 129, 178
Karachentsev, I. D., Karachentseva, V. E., & Huchtmeier, W. K. 2001, A&A, 366, 428
Karachentsev, I. D., Karachentseva, V. E., Huchtmeier, W. K., & Makarov, D. I. 2004, AJ, 127, 2031
Kreckel, K., Joung, M. R., & Cen, R. 2011, ApJ, 735, 132
Kreckel, K., Platen, E., Aragon-Calvo, M. A., et al. 2012, AJ, 144, 16
Lupton R., et al. 2005, `http://www.sdss.org/dr5/algorithms/sdssUBVRITransform.html#Lupton2005`
Makarov, D. I., Makarova, L. N., & Uklein, R. I. 2013, Astrophys. Bull., 68, 125
Matthews, L. D., & Uson, J. M. 2008, AJ, 135, 291
Matthews, L. D., & van Driel, W. 2000, A&AS, 143, 421
O'Neil, K. 2004, AJ, 128, 208
Patiri, S. G., Prada, F., Holtzman, J., Klypin, A., & Betancort-Rijo, J. 2006, MNRAS, 372, 1710
Paturel, G., Petit, C., Prugniel, P., et al. 2003, A&A, 412, 45
Perepelitsyna, Y. A., Pustilnik, S. A., & Kniazev, A. Y. 2014, Astrophys. Bull., 69, 247 (Paper IV)
Popping, A., & Braun, R. 2011, A&A, 528, A28
Pustilnik, S. A., & Martin, J.-M. 2007, A&A, 464, 859
Pustilnik, S. A., & Tepliakova, A. L. 2011, MNRAS, 414, 1188 (Paper I)
Pustilnik, S. A., Ugryumov, A. V., Lipovetsky, V. A., Thuan, T. X., & Guseva, N. G. 1995, ApJ, 443, 499
Pustilnik, S. A., Martin, J.-M., Huchtmeier, W., et al. 2002, A&A, 389, 405
Pustilnik, S. A., Tepliakova, A. L., Kniazev, A. Y., & Burenkov, A. N. 2010, MNRAS, 401, 333
Pustilnik, S. A., Tepliakova, A. L., & Kniazev, A. Y. 2011a, Astrophys. Bull., 66, 255 (Paper II)
Pustilnik, S. A., Martin, J.-M., Tepliakova, A. L., & Kniazev, A. Y. 2011b, MNRAS, 417, 1335 (Paper III)
Pustilnik, S. A., Perepelitsyna, Y. A., & Kniazev, A. Y., 2016, MNRAS, 463, 670 (Paper VII)
Rojas, R. R., Vogeley, M. S., Hoyle, F., & Brinkmann, J. 2004, ApJ, 617, 50
Rojas, R. R., Vogeley, M. S., Hoyle, F., & Brinkmann, J. 2005, ApJ, 624, 571
Schlafly, E. F., & Finkbeiner, D. P. 2011, ApJ, 737, 103
Schneider, S. E., Thuan, T. X., Magri, C., & Wadiak, J. E. 1990, ApJS, 72, 245
Schneider, S. E., Thuan, T. X., Mangum, J. G., & Miller, J. 1992, ApJS, 81, 5
Smoker, J. V., Davies, R. D., Axon, D. J., & Hummel, E. 2000, A&A, 361, 19
Sorrentino, G., Antonuccio-Delogu, V., & Rifatto, A. 2006, A&A, 460, 673
Springob, C. M., Haynes, M. P., Giovanelli, R., & Kent, B. R. 2005, ApJS, 160, 149
Staveley-Smith, L., Davies, R. D., & Kinman, T. D. 1992, MNRAS, 258, 334
Swaters, R. A., van Albada, T. S., van der Hulst, J. M., & Sancisi, R. 2002, A&A, 390, 863
Thuan, T. X., & Martin, G. E. 1981, ApJ, 247, 823
Thuan, T. X., Lipovetsky, V. A., Martin, J.-M., & Pustilnik, S. A. 1999, A&AS, 130, 100
Tully, R. B., Shaya, E. J., Karachentsev, I. D., et al. 2008, ApJ, 676, 184

Appendix A: Additional tables

Table A.1. Parameters of the Lynx-Cancer void sample galaxies observed with NRT.

Short IAU style name	Other name or prefix	Type	Coord. (2000.0)		$V_{\rm opt}$ km s^{-1}	V(HI) km s^{-1}	$B_{\rm tot}$‡ mag	$M^{0*}_{\rm B}$ mag	Alternative name
			RA h m s	Dec ° ′ ″					
(1)	(2)	(3)	(4)	(5)	(6)	(7)	(8)	(9)	(10)
J0626+2439	HIPASS	Scd	06 26 20.97	+24 39 20.0	1473 ± 7	1485 ± 2	17.98	–15.64	
J0629+2334	HIPASS	Scd	06 29 58.23	+23 34 28.5	1452 ± 6	1445 ± 3	17.10	–15.88	PGC 1689759
J0713+2926*	SDSS	dI?	07 13 05.15	+29 26 42.8	...	938 ± 2	16.79	–14.55	
J0723+3621	SDSS	Sm?	07 23 01.42	+36 21 17.1	888 ± 2	917 ± 2	17.01	–14.21	
J0723+3622	SDSS	LSB	07 23 13.46	+36 22 13.0	954 ± 3	970 ± 5	19.46	–11.76	
J0730+4109	SDSS	dI?	07 30 58.90	+41 09 59.8	874 ± 3	878 ± 5	16.67	–14.59	
J0737+4724	SDSS	LSB	07 37 28.47	+47 24 32.8	404 ± 60	474 ± 5	18.02	–12.54	
J0744+2508	SDSS	dI	07 44 43.72	+25 08 26.6	749 ± 4	760 ± 3	18.11	–12.66	
J0744+2506*	SDSS	dI	07 44 55.52	+25 06 01.8	778 ± 99	752 ± 6	20.47	–10.30	
J0747+5111	SDSS	Sm	07 47 32.10	+51 11 29.0	454 ± 84	433 ± 3	15.12	–15.16	MCG 9-13-56
J0802+0525[1]	SDSS	Comp	08 02 38.15	+05 25 51.2	830 ± 23	824 ± 6	19.80	–10.93	AGC 188988
J0809+4135	SDSS	Sd?	08 09 36.10	+41 35 40.0	704 ± 50	712 ± 5	15.46	–15.41	MCG 7-17-19
J0810+1837	SDSS	Sm:	08 10 30.65	+18 37 04.1	1495 ± 37	1481 ± 8	18.39	–13.58	
J0812+4836	SDSS	dI	08 12 39.53	+48 36 45.4	521 ± 5	522 ± 4	17.36	–13.08	
J0825+3201	SDSS	Ir	08 25 04.90	+32 01 05.1	648 ± 16	647 ± 6	16.91	–13.73	KUG 0821+321
J0831+4104	SDSS	LSB	08 31 41.21	+41 04 53.7	582 ± 40	640 ± 3	17.71	–12.92	
J0843+4025	SDSS	Im	08 43 37.98	+40 25 47.2	614 ± 3	627 ± 10	17.90	–12.68	
J0845+1519	SDSS	dI	08 45 25.40	+15 19 46.0	1642 ± 50	1584 ± 12	18.61	–13.40	
J0852+1350	SDSS	LSB	08 52 33.75	+13 50 28.3	1511 ± 4	1502 ± 8	17.40	–14.56	
J0859+3923	SDSS	dI	08 59 46.93	+39 23 05.6	588 ± 34	568 ± 3	17.25	–13.14	
J0900+3222*	SDSS	dI	09 00 18.30	+32 22 26.2	740 ± 30	...	18.97	–11.77	
J0911+3135	SDSS	dI	09 11 59.43	+31 35 35.9	750 ± 4	753 ± 6	18.05	–12.68	
J0917+2525	IC2450	S0	09 17 05.27	+25 25 44.9	1644 ± 2	1643 ± 12	14.06	–18.11	
J0926+3343	SDSS	Sm:	09 26 09.45	+33 43 04.1	565 ± 57	536 ± 2	17.30	–12.91	
J0928+2845	SDSS	dI	09 28 59.06	+28 45 28.5	1229 ± 41	1224 ± 7	16.76	–14.82	
J0929+1155	SDSS	dI	09 29 51.83	+11 55 35.7	1641 ± 6	1614 ± 8	17.20	–14.84	
J0931+2717	SDSS	Sm:	09 31 36.15	+27 17 46.6	1505 ± 2	1504 ± 3	18.00	–13.94	
J0934+0625*	CGCG035-007	Sc	09 34 44.72	+06 25 31.2	574 ± 38	548 ± 4	15.42	–14.50	
J0937+2733	SDSS	Im	09 37 47.65	+27 33 57.7	1595 ± 16	1588 ± 1	16.50	–15.58	
J0940+4459	SDSS	dI	09 40 03.27	+44 59 31.7	1358 ± 4	1350 ± 10	18.01	–13.79	
J0942+0937*	SDSS	dI	09 42 51.25	+09 37 57.6	1461 ± 17	1456 ± 6	18.15	–13.67	
J0943+4134	SDSS	dI	09 43 42.97	+41 34 08.9	1403 ± 40	1436 ± 4	17.64	–14.25	
J0944+1000	SDSS	dI	09 44 37.10	+10 00 46.3	1477 ± 66	1476 ± 3	16.96	–14.89	
J0947+4138	SDSS	BCG	09 47 18.35	+41 38 16.4	1389 ± 2	1400 ± 2	17.92	–13.93	HS 0944+4152
J0947+3905a*	MRK407	BCG	09 47 47.60	+39 05 03.0	1589 ± 10	1582 ± 4	15.28	–16.79	
J0947+3908*	UZC	Sd	09 47 50.25	+39 08 31.7	1553 ± 25	1565 ± 4	16.85	–15.20	
J0947+3905b	SDSS	LSB	09 47 58.45	+39 05 10.1	1501 ± 60	1567 ± 4	18.03	–14.02	
J0951+3842	SDSS	dI	09 51 41.67	+38 42 07.3	1435 ± 4	1433 ± 7	17.46	–14.43	
J0954+3620	SDSS	dI	09 54 50.60	+36 20 01.9	503 ± 55	550 ± 5	18.05	–12.17	
J0956+2716*	SDSS	dI	09 56 33.65	+27 16 59.3	1074 ± 25	1059 ± 2	18.13	–13.17	
J0957+2745*	SDSS	dI	09 57 29.40	+27 45 24.3	1184 ± 16	1184 ± 4	18.16	–13.33	
J0959+4736	SDSS	dI	09 59 18.60	+47 36 58.4	1093 ± 4	1110 ± 12	17.05	–14.37	PC 0956+4751
J1000+3032	SDSS	dI	10 00 36.54	+30 32 09.8	501 ± 37	484 ± 13	18.14	–11.87	
J1010+4617	SDSS	dI	10 10 14.96	+46 17 44.1	1092 ± 3	1092 ± 3	18.23	–13.15	
J1019+2923	SDSS	dI	10 19 28.52	+29 23 02.3	874 ± 43	885 ± 4	17.48	–13.60	

Notes. (1) Probable artifact. See text in Sect. 4.

Table A.2. HI parameters of the observed Lynx-Cancer void sample galaxies.

Short IAU style name (1)	V(HI)±σ km s^{-1} (2)	Dist adopt (3)	W_{50} ± σ km s^{-1} (4)	W_{20} ± σ km s^{-1} (5)	F(HI)±σ Jy km s^{-1} (6)	log ±σ M(HI) (7)	$\frac{M(\mathrm{HI})\pm\sigma}{L_B}$ (8)	Time min (9)	rms mJy (10)	S/N (11)
J0626+2439	1485 ± 2	23.21	138 ± 3	156 ± 5	7.04 ± 0.22	8.95 ± 0.013	3.20 ± 0.100	42	3.5	16.2
J0629+2324	1445 ± 2	22.92	129 ± 3	150 ± 4	10.40 ± 0.25	9.11 ± 0.010	3.69 ± 0.090	22	4.1	22.2
J0713+2926	938 ± 2	16.10	40 ± 3	61 ± 4	1.57 ± 0.06	7.98 ± 0.016	0.93 ± 0.035	80	1.6	24.0
J0723+3621*	917 ± 1	16.00	100 ± 4	122 ± 6	3.74 ± 0.18	8.35 ± 0.021	2.93 ± 0.143	64	3.4	17.2
J0723+3622*	970 ± 1	16.00	45 ± 10	69 ± 16	1.59 ± 0.16	7.98 ± 0.041	11.89 ± 1.189	49	3.8	7.0
J0730+4109	878 ± 5	15.75	51 ± 10	72 ± 16	0.74 ± 0.10	7.64 ± 0.056	0.41 ± 0.056	84	2.4	6.0
J0737+4724	474 ± 5	10.40	40 ± 4	53 ± 6	0.99 ± 0.09	7.40 ± 0.037	1.58 ± 0.140	117	2.4	10.8
J0744+2508	760 ± 3	13.10	28 ± 6	43 ± 9	0.39 ± 0.05	7.20 ± 0.052	0.88 ± 0.113	128	1.7	7.5
J0744+2506	752 ± 6	13.10	22 ± 12	34 ± 19	0.032 ± 0.016	6.11 ± 0.176	0.64 ± 0.320	140	1.6	2.9
J0747+5111	433 ± 3	9.92	75 ± 5	105 ± 9	5.96 ± 0.27	8.14 ± 0.019	0.77 ± 0.035	26	5.2	15.4
J0802+0527	830 ± 6	13.25	...	...	0.10 ± 0.10	<6.62 ± 0.301	<1.14 ± 1.140	69	2.8	2.0
J0809+4135	712 ± 5	13.48	95 ± 10	137 ± 16	5.13 ± 0.30	8.34 ± 0.025	0.97 ± 0.057	19	5.1	12.0
J0810+1837	1481 ± 8	23.03	42 ± 15	64 ± 24	0.46 ± 0.09	7.76 ± 0.079	1.37 ± 0.274	25	2.3	4.4
J0812+4836	522 ± 4	11.04	47 ± 8	64 ± 12	1.27 ± 0.18	7.56 ± 0.057	1.38 ± 0.192	166	4.4	6.5
J0825+3201	647 ± 6	12.23	62 ± 12	84 ± 18	1.11 ± 0.17	7.59 ± 0.062	0.82 ± 0.126	37	3.7	5.6
J0831+4104	640 ± 3	12.44	25 ± 6	32 ± 9	0.17 ± 0.06	6.79 ± 0.135	0.27 ± 0.098	92	2.2	3.5
J0843+4025	627 ± 10	12.23	24 ± 21	46 ± 33	0.19 ± 0.09	6.83 ± 0.168	0.37 ± 0.175	63	2.8	3.2
J0845+1519	1584 ± 12	24.19	6 ± 24	39 ± 38	0.10 ± 0.05	7.14 ± 0.176	0.39 ± 0.195	175	1.6	4.1
J0852+1350	1502 ± 8	22.96	77 ± 15	118 ± 24	2.30 ± 0.22	8.46 ± 0.039	2.75 ± 0.261	20	4.0	8.0
J0859+3923	568 ± 3	11.36	31 ± 7	46 ± 11	0.60 ± 0.09	7.26 ± 0.064	0.65 ± 0.103	54	2.8	6.5
J0900+3222	740 ± 30	13.18	...	...	0.14 ± 0.10	<6.76 ± 0.231	<0.72 ± 0.520	35	3.4	1.4
J0911+3135	753 ± 6	13.56	27 ± 12	52 ± 18	0.48 ± 0.07	7.32 ± 0.061	1.14 ± 0.171	85	2.0	6.5
J0917+2525	1643 ± 12	25.45	98 ± 24	131 ± 38	0.81 ± 0.16	8.09 ± 0.079	0.05 ± 0.010	23	2.8	4.1
J0926+3343	536 ± 2	10.63	43 ± 4	79 ± 7	2.71 ± 0.10	7.86 ± 0.015	3.23 ± 0.117	72	2.2	24.4
J0928+2845	1224 ± 7	19.84	94 ± 14	123 ± 22	1.99 ± 0.26	8.27 ± 0.053	1.41 ± 0.182	17	4.6	6.3
J0929+1155	1614 ± 8	24.29	119 ± 15	138 ± 24	3.14 ± 0.17	8.64 ± 0.023	3.27 ± 0.178	37	2.9	3.7
J0931+2717	1504 ± 3	23.59	48 ± 6	71 ± 10	0.54 ± 0.13	7.85 ± 0.092	1.21 ± 0.285	47	3.0	11.0
J0934+0625	548 ± 4	8.88	86 ± 8	116 ± 12	4.07 ± 0.22	7.88 ± 0.023	0.77 ± 0.042	34	4.1	11.4
J0937+2733	1588 ± 1	25.08	33 ± 2	52 ± 3	3.04 ± 0.12	8.66 ± 0.016	1.71 ± 0.065	38	3.2	27.1
J0940+4459	1350 ± 10	22.25	30 ± 16	50 ± 25	0.11 ± 0.05	7.11 ± 0.163	0.25 ± 0.114	77	2.8	1.3
J0942+0937	1456 ± 6	21.93	43 ± 13	63 ± 20	0.55 ± 0.05	7.80 ± 0.041	1.37 ± 0.137	26	2.4	5.0
J0943+4134	1436 ± 4	23.33	46 ± 9	64 ± 13	0.43 ± 0.06	7.74 ± 0.060	0.70 ± 0.104	71	1.6	6.3
J0944+1000	1476 ± 3	22.21	64 ± 6	87 ± 9	2.23 ± 0.14	8.41 ± 0.027	1.84 ± 0.116	21	3.0	12.1
J0947+4138	1400 ± 2	22.71	61 ± 3	90 ± 5	0.20 ± 0.07	7.39 ± 0.132	0.42 ± 0.149	132	1.5	27.9
J0947+3905a	1582 ± 4	25.11	157 ± 7	193 ± 12	7.00 ± 0.50	9.02 ± 0.030	1.29 ± 0.092	22	3.3	27.0
J0947+3908	1565 ± 4	25.11	...	...	5.00 ± 0.40	8.87 ± 0.033	3.92 ± 0.314	20	3.0	22.0
J0947+3905b	1567 ± 4	25.11	...	...	1.50 ± 0.20	8.35 ± 0.054	3.48 ± 0.464	20	3.0	21.0
J0951+3842	1433 ± 7	23.04	29 ± 14	56 ± 22	0.48 ± 0.11	7.78 ± 0.089	0.65 ± 0.148	48	2.9	5.7
J0954+3620	550 ± 5	10.86	44 ± 10	63 ± 15	0.28 ± 0.05	6.89 ± 0.074	0.68 ± 0.126	86	1.3	6.0
J0956+2716**	1059 ± 2	19.94	56 ± 5	68 ± 8	1.46 ± 0.12	8.14 ± 0.035	1.90 ± 0.161	44	3.0	10.9
J0957+2745	1184 ± 4	19.14	40 ± 9	52 ± 13	0.33 ± 0.07	7.46 ± 0.086	0.86 ± 0.188	45	2.1	4.2
J0959+4736	1110 ± 12	18.89	80 ± 24	134 ± 37	1.91 ± 0.16	8.21 ± 0.036	1.80 ± 0.154	47	3.6	6.8
J1000+3032	484 ± 13	9.68	34 ± 25	55 ± 39	0.15 ± 0.07	6.52 ± 0.166	0.38 ± 0.177	29	2.5	3.0
J1010+4617	1092 ± 3	18.57	...	...	0.06 ± 0.06	<6.69 ± 0.301	<0.34 ± 0.340	37	2.4	2.0
J1019+2923	885 ± 4	15.40	71 ± 8	86 ± 12	1.04 ± 0.13	7.77 ± 0.051	1.36 ± 0.170	23	2.8	5.8

Notes. (*) HI parameters are adopted based on GMRT data from Chengalur & Pustilnik (2013); (**) distance as for IC2520 = J0956+2713, a massive component of pair with $V_{\mathrm{hel}} = 1243$ km s^{-1}.

Table A.3. Lynx-Cancer void sample galaxies with HI data from literature.

Short IAU style name (1)	Other name or prefix (2)	Type (3)	Coord. (2000.0)		$V_{\rm hel}$ km s^{-1} (6)	$B_{\rm tot}$ mag (7)	$M^{0*}_{\rm B}$ mag (8)	F(HI) Jy km s^{-1} (9)	M(HI) $L_{\rm B}$ (sun) (10)	Source of HI (11)
			RA h m s (4)	Dec ° ′ ″ (5)						
J0630+3930	UGC3475	Sm	06 30 28.86	+39 30 13.6	487	14.97	–15.88	24.60	1.76	HR89
J0630+3318	UGC3476	Im	06 30 29.22	+33 18 07.2	469	14.96	–16.02	12.51	0.72	Sch92
J0638+2239	UGC3503	Sd	06 38 01.40	+22 39 06.0	1389	15.10	–17.28	9.66	0.89	Sp05
J0838+4915	UGC3501	Im:	06 38 38.40	+49 15 30.0	449	17.20	–13.32	3.60	2.62	HR89
J0643+2252	UGC3516	Sd	06 43 08.51	+22 52 24.9	1287	16.97	–15.77	2.81	0.88	Sch90
J0647+4730	KKH 38	I	06 47 54.88	+47 30 50.0	451	17.40	–12.98	6.50	6.25	KKH01
J0653+1917	UGC3587	S?	06 53 54.70	+19 17 59.0	1267	13.84	–18.08	49.57	1.80	Sp05
J0655+3905	UGC3600	Im:	06 55 40.00	+39 05 42.8	412	15.92	–14.21	5.50	1.49	Sch92
J0706+3020*	SDSS	LSB	07 06 23.43	+30 20 51.3	937	19.10	–12.36	3.41	17.10	CPE16
J0706+3019	UGC3672	Im	07 06 27.56	+30 19 19.4	994	15.92	–15.54	11.94	3.15	CPE16
J0709+4422	UGC3698	Im	07 09 16.8	+44 22 48.0	422	15.41	–14.96	7.95	1.20	Sw02
J0710+4427	NGC2337	IBm	07 10 13.6	+44 27 25.0	436	13.48	–16.85	38.00	1.00	Sw02
J0713+1031*	UGC3755	Im	07 13 51.80	+10 31 19.0	315	14.07	–15.66	10.56	0.48	Sp05
J0722+4506	UGC3817	Im	07 22 44.48	+45 06 30.7	437	15.96	–14.44	10.20	2.50	Sw02
J0723+3624*	SDSS	LSB	07 23 20.57	+36 24 40.8	938	21.68	–9.56	0.48	28.30	CP13
J0725+0910	PGC020981	I	07 25 38.95	+09 10 59.8	1202	16.69	–14.94	1.80	1.01	AL11
J0727+4826	UGC3853	Sdm	07 27 39.26	+48 26 45.4	936	15.96	–15.63	4.60	1.11	MV00
J0728+4046	UGC3860	Im	07 28 17.2	+40 46 13.0	354	15.21	–14.50	11.76	1.72	Beg08
J0729+2754	UGC3876	SAd	07 29 17.49	+27 54 01.9	854	13.77	–17.30	18.70	0.77	HR89
J0734+0432	UGC3912	IBm:	07 34 12.63	+04 32 47.1	1240	14.72	–16.87	14.39	1.37	Sp05
J0736+0959*	AGC174585	–	07 36 10.30	+09 59 11.0	357	17.90	–11.54	0.54	1.01	AL11
J0741+4006	UGC3966	Im	07 41 26.00	+40 06 44.0	361	15.32	–14.58	25.10	4.18	Sw02
J0741+1648*	DDO47	IBsm	07 41 55.00	+16 48 02.0	272	14.89	–14.78	64.00	7.73	Sp05
J0742+1633*	KK65	dIrr	07 42 31.20	+16 33 40.0	279	15.51	–14.15	2.50	0.53	Beg08
J0743+0357*	CGCG030-012	Sdm:	07 43 08.77	+03 57 00.0	932	15.60	–15.41	3.66	0.82	AL11
J0746+5117	MCG9-13-52	Sm	07 46 56.36	+51 17 42.8	445	16.54	–13.75	2.60	1.27	KKH01
J0757+1423*	UGC4115	IAm	07 57 01.80	+14 23 27.0	341	14.81	–14.75	21.60	2.47	Beg08
J0757+3556	UGC4117	IBm	07 57 25.98	+35 56 21.0	773	15.36	–15.59	5.04	0.89	ONe04
J0800+4211	UGC4148	Sm	08 00 23.68	+42 11 37.0	716	15.66	–15.18	12.50	2.98	Sp05
J0801+5044	NGC2500	SBd	08 01 53.30	+50 44 15.4	504	12.14	–18.21	34.60	0.32	Sp05
J0813+4559	NGC2537	BCG	08 13 14.73	+45 59 26.3	445	12.49	–17.71	21.10	0.26	MU08
J0813+4544	IC2233	Sd	08 13 58.93	+45 44 34.3	553	13.34	–17.03	47.60	1.29	MU08
J0814+4903	NGC2541	Scd	08 14 40.18	+49 03 42.1	548	12.34	–18.36	135.60	1.67	Sp05
J0819+5000	NGC2552	SAm	08 19 20.14	+50 00 25.2	524	13.01	–17.42	28.50	0.58	Sp05
J0825+3532	HS0822+3542	BCG	08 25 55.43	+35 32 31.9	720	17.88	–12.97	0.34	0.61	Ch06
J0826+3535	SAO0822+3545	Im	08 26 05.59	+35 35 25.7	740	17.74	–13.11	1.00	1.58	Ch06
J0826+2145*	SDSS	dI	08 26 20.01	+21 45 22.8	420	18.23	–11.63	0.46	1.16	PMM16
J0828+4151	DDO52	Im	08 28 28.53	+41 51 22.8	397	15.35	–14.87	10.80	1.96	Sp05
J0859+3912	UGC4704	Sdm	08 59 00.28	+39 12 35.7	596	14.82	–15.66	22.40	2.56	HR89
J0900+2536	UGC4722	Sdm	09 00 23.54	+25 36 40.6	1795	15.01	–17.39	11.6	1.25	Ch15
J0900+2538*	UGC4722C	dI	09 00 26.11	+25 38 21.4	1837	17.21	–15.19	4.30	4.30	Ch15
J0908+0517	KKH46	dI	09 08 36.54	+05 17 26.8	598	17.21	–12.99	3.07	2.98	AL11
J0929+2502	SDSS	dI	09 29 00.10	+25 02 57.0	1661	19.03	–13.16	0.36	2.38	AL11
J0940+2935	KISSB23	Im	09 40 12.67	+29 35 29.3	507	16.32	–13.53	2.20	1.03	PM07
J0942+3316	UGC5186	Im	09 42 59.10	+33 16 00.2	551	15.99	–14.23	1.40	0.50	Beg08
J0943+3326	AGC198691	dI	09 43 32.35	+33 26 57.6	514	19.82	–10.40	0.53	6.46	Hir16
J0944+0936*	IC559	Sc	09 44 43.90	+09 36 55.0	541	14.77	–15.22	5.33	0.59	PB11
J0945+3214	UGC5209	Im	09 45 04.20	+32 14 18.2	538	16.07	–14.08	1.53	0.73	KKH01
J0950+3127	UGC5272b	Im	09 50 19.49	+31 27 22.3	541	17.56	–12.60	1.16	1.70	Sw02
J0950+3129	UGC5272	Im	09 50 22.40	+31 29 16.0	520	14.45	–15.71	19.30	1.61	Sw02
J0951+0749*	UGC5288	Sdm?	09 51 17.20	+07 49 38.0	556	14.62	–15.61	25.30	1.96	PB11
J0956+2716*	IC2520	S	09 56 20.40	+27 13 39.0	1243	14.27	–17.32	6.04	0.43	HR89
J0956+2900*	DDO68C	dI	09 56 41.07	+29 00 50.7	506	17.48	–13.12	0.73	1.00	Can14
J0956+2849	DDO68A	Im	09 56 45.70	+28 49 35.0	502	14.70	–15.90	26.70	2.86	Ek08
J0958+4744*	UGC5354	Sm	09 58 53.40	+47 44 13.0	1168	14.15	–17.39	19.91	1.30	Sp05
J1004+2921	UGC5427	Sdm	10 04 41.05	+29 21 55.2	495	14.91	–15.50	1.85	0.23	Sch90
J1008+2932	UGC5464	Sm	10 08 07.65	+29 32 30.5	1011	15.77	–15.47	2.86	0.81	Sch90
J1016+3746	UGC5540	Sc	10 16 21.7	+37 46 48.7	1166	14.63	–16.85	5.37	0.54	PM07
J1016+3754	HS1013+3809	BCG	10 16 24.5	+37 54 46.0	1173	16.02	–15.46	1.51	0.86	PM07

References. (*) Galaxy from the updated sample; HR89: Huchtmeier & Richter (1989); Sch90: Schneider et al. (1990); Sch92: Schneider et al. (1992); Sp05: Springob et al. (2005); KKH01: Karachentsev et al. (2001); Sw02: Swaters et al. (2002); MV00: Matthews & van Driel (2000); CP13: Chengalur & Pustilnik (2013); AL11: Haynes et al. (2011); Beg08: Begum et al. (2008); ONe04: O'Neil (2004); MU08: Matthews & Uson (2008); Ch06: Chengalur et al. (2006); PMM16: Pustilnik et al. (2016); Ch15: Chengalur et al. (2015); Can14: Cannon et al. (2014); PM07: Pustilnik & Martin (2007); Hir16: Hirschauer et al. (2016); PB11: Popping & Braun (2011); CPE16: Chengalur et al. (2016).